Received September 2001
Accepted May 2002

Numerical calculation of developing laminar flow in rotating ducts with a 180° bend

F. Papa
Department of Chemical Engineering, University of Toledo, Toledo, USA

T.G. Keith, Jr. and K.J. DeWitt
Department of Mechanical Engineering, University of Toledo, Toledo, USA

K. Vaidyanathan
Federal-Mogul Co., Ann Arbor, USA

Keywords *Rotating flows, Laminar flow, Numerical methods*

Abstract *This study is concerned with developing laminar flow of an incompressible, Newtonian fluid, having constant viscosity, rotating in circular and rectangular ducts that contain a 180° bend. The Reynolds number ranges from 100 to 400, the rotation number from 0 to 0.4, and the Dean number from 66 to 264. Positive and negative rotation modes are considered. The artificial compressibility method is used for the numerical calculations and new boundary conditions are developed for these flows. It is shown that rotation causes the secondary flow to occur in ducts of any geometry, and that the strength of the secondary flow in the bend due to both rotation and curvature decreases as compared to the no rotation case.*

Introduction

Fluid flow in curved ducts undergoing orthogonal rotation has several applications in practical engineering problems. Orthogonal rotation for this geometry is where the axis of rotation is parallel to the axis of curvature of the duct, as shown in Figure 1. Examples where this type of flow occurs are lubricants in internal combustion engine passages, fluids in cooling systems, air in turbo-machinery passages, as well as blood flow when the human body is subjected to rotation.

Laminar flow in conduits has been widely studied in the past. Hagen in 1839 and Poiseuille in 1840 obtained the classical parabolic solution for one-dimensional laminar flow in stationary, straight circular ducts. This one-dimensional Hagen-Poiseuille laminar flow becomes a three-dimensional flow if the circular duct is subjected to orthogonal rotation. Barua (1955) and Benton

The results presented in this paper were obtained in the course of research sponsored by Federal Mogul Corporation.

International Journal of Numerical Methods for Heat & Fluid Flow, Vol. 12 No. 7, 2002, pp. 780-799.

DOI 10.1108/09615530210443025

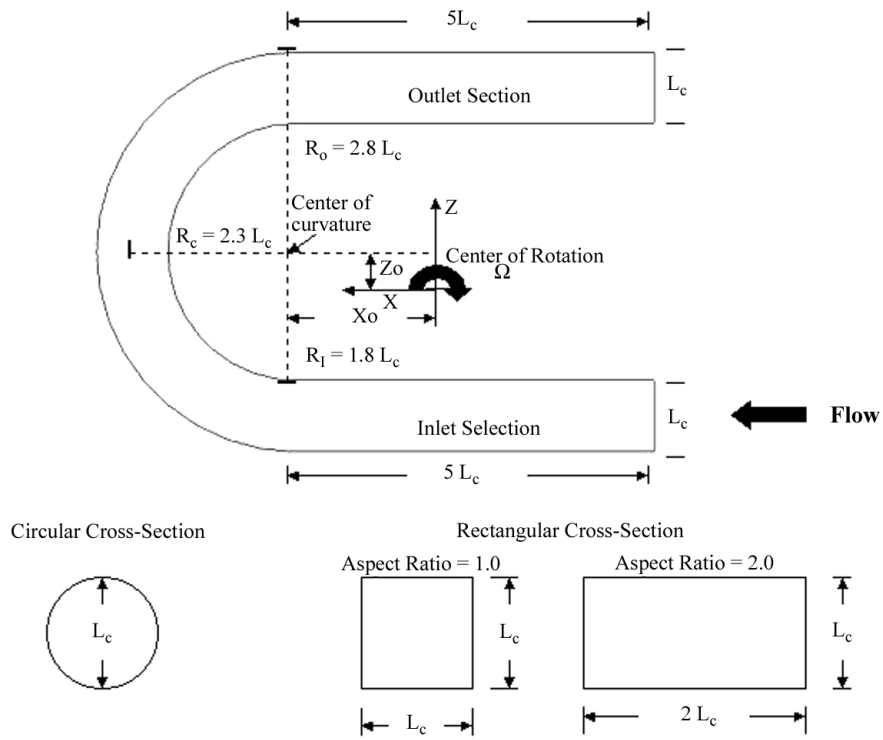

Figure 1.
Flow configuration and coordinate system

(1956) studied the flow in a straight circular duct rotating at a constant angular velocity about an axis perpendicular to the main flow direction in the duct (orthogonal rotation). Their solutions are only valid for small angular velocity because the authors assumed perturbations on the Hagen-Poiseuille flow.

Speziale (1982, 1986) numerically solved the case of laminar flow in a straight rectangular duct under orthogonal rotation. The duct was considered long enough that the end effects could be neglected. The governing equations in a Cartesian coordinate system were solved using finite differences and the streamfunction-vorticity method. Because of the coordinate system used, only rectangular ducts were analyzed.

The first solution of the flow in a stationary curved circular duct was offered by Dean (1928), who showed that the centrifugal force due to the curvature would push the peak of the main velocity towards the outer wall of the bend, thus producing a double-spiral secondary flow. Dean established a non-dimensional parameter to describe the phenomenon, the Dean number,

$$K = \mathrm{Re}\left(\frac{L_c}{R_c}\right)^{\frac{1}{2}} \quad \text{and} \quad \mathrm{Re} = \frac{L_c \bar{W}}{v} \tag{1}$$

where Re is the Reynolds number, L_c a characteristic length, R_c the curvature radius, $\bar{W}$ the average axial velocity, and v the fluid kinematic viscosity.

Flows in straight ducts under orthogonal rotation are characterized by the presence of secondary flow, consisting of a pair of counter-rotating vortices, as shown in Figure 2 for a circular duct. As the fluid density is considered constant, the centrifugal force acts as a conservative force and only the Coriolis force generates the secondary flow. The rotational effect is taken into account using a non-dimensional parameter known as the rotation number, Ro, and defined as the ratio of the Coriolis force to the inertial force, i.e.

$$\mathrm{Ro} = \frac{\Omega L_c}{\bar{W}} \tag{2}$$

where Ω is the angular rate of rotation.

Many authors, such as Daskopoulos and Lenhoff (1990), Selmi *et al.* (1994) and Iacovides *et al.* (1996) have studied the flow in curved ducts under orthogonal rotation, where the axis of rotation is parallel to the axis of curvature of the duct (perpendicular to the main flow direction in the duct). In these works a fully developed flow along the bend (independent of angular coordinate) is assumed. Ito and Motal (1974) showed that the centrifugal force present due to the bend curvature always acts radially outwards along the bend irrespective of the direction of rotation. The Coriolis force acts perpendicular to the axis of rotation, but its direction can be radially outwards or inwards for positive or negative rotation, respectively. Most recently, Hwang

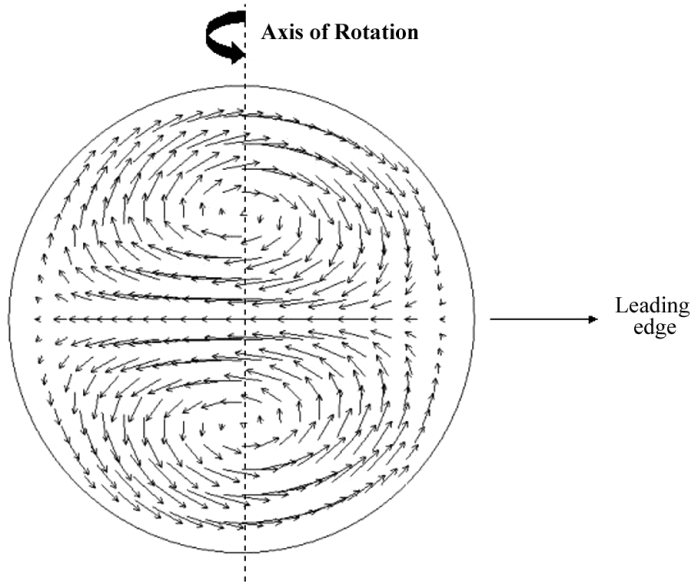

Figure 2.
Typical secondary flow pattern for rotating laminar flow

and Lai (1998a, b) studied the three-dimensional flow problems in rotating multiple-pass square channels.

In the present work, numerical results are obtained for the developing laminar flow in ducts having circular or rectangular cross-sections, a 180° bend, and are rotating either positively or negatively about an axis parallel to the axis of curvature of the duct (orthogonal rotation). Rectangular ducts with aspect ratios (height to width) of 1.0 and 2.0 and circular ducts with a diameter equal to the characteristic length are considered. The Dean numbers ranged from 65.94 to 263.75, rotation numbers from 0.0 to 0.4 and Reynolds numbers from 100 to 400.

Formulation of the physical problem

Figure 1 shows the geometry and dimensions of the 180° bend used in this study. The characteristic length is the duct height and the rectangular cross-sections have aspect ratios of 1.0 or 2.0. The inlet and outlet sections were located at a distance five times the characteristic length from the bend, and the radius of curvature along the bend is 2.3 times its characteristic length. The bend rotates at a constant angular rate of rotation Ω about an axis, which is parallel to the curvature axis. Because the Coriolis force direction can act radially outwards or inwards along the bend, it is necessary to define two different rotational modes called positive or negative rotation. Positive rotation is when the bend shown in Figure 1 rotates in a clockwise direction and therefore, the Coriolis force acts radially outwards along the bend. Negative rotation is when the bend shown in Figure 1 is under counter-clockwise rotation and the Coriolis force acts radially inwards along the bend. The fluid is considered incompressible and Newtonian with constant properties, and the flow is considered steady.

The 180° bend under rotation represents a non-inertial frame of reference because its acceleration will cause "fictitious forces" not considered in classical flow problems. The governing equations used in flow modeling must be modified to consider these new forces due to rotation, which comprised centrifugal and Coriolis forces. As previously mentioned, the fluid is assumed incompressible and therefore, the centrifugal force due to rotation is conservative. As a result, the static pressure and the potential of the centrifugal force can be coupled together using a modified pressure, and the calculated velocity field is independent of the distance from the axis of rotation to the axis of curvature (X_o, Z_o in Figure 1).

The governing equations, with respect to the x, y, and z coordinate system (Figure 3a) are

Continuity

$$\frac{\partial u}{\partial x}+\frac{\partial v}{\partial y}+\frac{\partial w}{\partial z}=0 \tag{3}$$

Momentum

x-component

$$\rho\left(\frac{\partial u}{\partial t}+u\frac{\partial u}{\partial x}+v\frac{\partial u}{\partial y}+w\frac{\partial u}{\partial z}\right)=-\frac{\partial P}{\partial x}+\mu\left(\frac{\partial^2 u}{\partial x^2}+\frac{\partial^2 u}{\partial y^2}+\frac{\partial^2 u}{\partial z^2}\right)-2\rho\Omega w \quad (4)$$

y-component

$$\rho\left(\frac{\partial v}{\partial t}+u\frac{\partial v}{\partial x}+v\frac{\partial v}{\partial y}+w=\frac{\partial v}{\partial z}\right)=-\frac{\partial P}{\partial y}+\mu\left(\frac{\partial^2 v}{\partial x^2}+\frac{\partial^2 v}{\partial y^2}+\frac{\partial^2 v}{\partial z^2}\right) \quad (5)$$

z-component

$$\rho\left(\frac{\partial w}{\partial t}+u\frac{\partial w}{\partial x}+v\frac{\partial w}{\partial y}+w\frac{\partial w}{\partial z}\right)=-\frac{\partial P}{\partial z}+\mu\left(\frac{\partial^2 w}{\partial x^2}+\frac{\partial^2 w}{\partial y^2}+\frac{\partial^2 w}{\partial z^2}\right)+2\rho\Omega u \quad (6)$$

where, u, v, and w are the velocity components in the x, y, and z directions, respectively. The quantity P is the modified pressure, which simplifies the momentum equations in a rotating coordinate system and is defined as:

$$P=p+\rho\Phi \quad \text{where} \quad \Phi=\frac{\Omega^2}{2}(x^2+z^2) \quad (7)$$

Note that the modified pressure includes the static pressure (p) and the potential of the centrifugal term (Φ). This form of simplification can be made because the fluid density is constant.

Equations (3)-(6) are given in dimensionless form using a reference length and reference velocity. The reference velocity used is the average axial velocity, $\bar{W}$. The reference length used is the circular diameter and the rectangular height, L_c, as explained in Figure 1.

The dimensionless quantities obtained are:

$$x^*=\frac{x}{L_c} \quad y^*=\frac{y}{L_c} \quad z^*=\frac{z}{L_c} \quad u^*=\frac{u}{\bar{W}} \quad v^*=\frac{v}{\bar{W}}$$

$$w^*=\frac{w}{\bar{W}} \quad P^*=\frac{P}{\rho W^2} \quad t^*=\frac{t\bar{W}}{L_c} \quad \mathrm{Ro}=\frac{\Omega L_c}{\bar{W}}$$

Using these quantities, the dimensionless form of equations (3)-(6) are obtained as:

$$\frac{\partial u^*}{\partial x^*}+\frac{\partial v^*}{\partial y^*}+\frac{\partial w^*}{\partial z^*}=0 \quad (8)$$

$$\frac{\partial u^*}{\partial t^*} + u^* \frac{\partial u^*}{\partial x^*} + v^* \frac{\partial u^*}{\partial y^*} + w^* \frac{\partial u^*}{\partial z^*} = -\frac{\partial P^*}{\partial x^*} + \frac{1}{\mathrm{Re}} \left(\frac{\partial^2 u^*}{\partial x^{*2}} + \frac{\partial^2 u^*}{\partial y^{*2}} + \frac{\partial^2 u^*}{\partial z^{*2}} \right) - 2\mathrm{Ro}\, w^* \tag{9}$$

$$\frac{\partial v^*}{\partial t^*} + u^* \frac{\partial v^*}{\partial x^*} + v^* \frac{\partial v^*}{\partial y^*} + w^* \frac{\partial v^*}{\partial z^*} = -\frac{\partial P^*}{\partial y^*} + \frac{1}{\mathrm{Re}} \left(\frac{\partial^2 v^*}{\partial x^{*2}} + \frac{\partial^2 v^*}{\partial y^{*2}} + \frac{\partial^2 v^*}{\partial z^{*2}} \right) \tag{10}$$

$$\frac{\partial w^*}{\partial t^*} + u^* \frac{\partial w^*}{\partial x^*} + v^* \frac{\partial w^*}{\partial y^*} + w^* \frac{\partial w^*}{\partial z^*} = -\frac{\partial P^*}{\partial z^*} + \frac{1}{\mathrm{Re}} \left(\frac{\partial^2 w^*}{\partial x^{*2}} + \frac{\partial^2 w^*}{\partial y^{*2}} + \frac{\partial^2 w^*}{\partial z^{*2}} \right) + 2\mathrm{Ro}\, u^* \tag{11}$$

This set of equations contains two non-dimensional parameters: the Reynolds number and the rotation number. The Dean number is calculated using equation (1).

Numerical procedure

Equations (8)-(11) are coupled, non-linear, partial differential equations. Clearly, an analytical solution of this set of equations is not possible. Even the task of solving them numerically is enormous, requiring complicated boundary conditions that must remain valid under a rotating frame of reference. Also, because the fluid is incompressible, it is necessary to find a method to link changes in the velocity field to changes in the pressure field.

The domain studied in this work is represented using a boundary-fitted coordinate system, and the governing equations are solved in a transformed hexahedral computational domain. Figure 3(a) shows the grid for the 180° bend with a circular cross-section in the physical domain, and Figure 3(b) is the representation of the same geometry in the computational domain. The set of

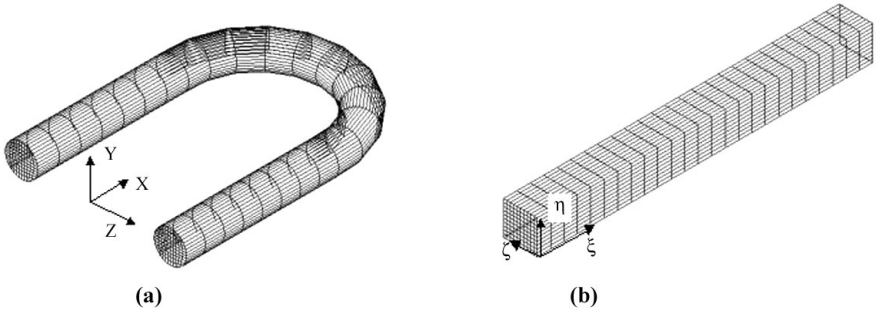

Figure 3.
(a) 180° bend with circular cross-section on physical domain; (b) 180° bend with circular cross-section on computational domain

governing equations can be written in non-dimensional vector form for a generalized coordinate system as

$$\frac{\partial}{\partial t}(\hat{D}) + \frac{\partial}{\partial \xi}(\hat{E}_c - \hat{E}_v) + \frac{\partial}{\partial \eta}(\hat{F}_c - \hat{F}_v) + \frac{\partial}{\partial \zeta}(\hat{G}_c - \hat{G}_v) = \hat{S} \tag{12}$$

where

$$\hat{D} = \begin{bmatrix} \rho^* \\ u^* \\ v^* \\ w^* \end{bmatrix} \tag{13}$$

The quantity ρ^* is an artificial density and is related to the modified pressure by the artificial equation of state

$$P^* = \frac{\rho^*}{\beta} \tag{14}$$

where β is the artificial compressibility factor. The convective vectors are

$$\hat{E}_c = \frac{1}{J}\begin{bmatrix} U \\ u^*U + P^*\xi_X \\ v^*U + P^*\xi_Y \\ w^*U + P^*\xi_Z \end{bmatrix} \quad \hat{F}_c = \frac{1}{J}\begin{bmatrix} V \\ u^*V + P^*\eta_X \\ v^*V + P^*\eta_Y \\ w^*W + P^*\eta_Z \end{bmatrix} \quad \hat{G}_c = \frac{1}{J}\begin{bmatrix} W \\ u^*W + P^*\zeta_X \\ v^*W + P^*\zeta_Y \\ w^*W + P^*\zeta_Z \end{bmatrix} \tag{15}$$

and U, V, W are

$$\begin{aligned} U &= \xi_x U^* + \xi_y V^* + \xi_z W^* \\ V &= \eta_x U^* + \eta_y V^* + \eta_z W^* \\ W &= \zeta_x U^* + \zeta_y V^* + \zeta_z W^* \end{aligned} \tag{16}$$

The quantity J is the Jacobian of the transformation defined as the determinant of the Jacobian matrix:

$$J = \frac{(x^*, y^*, z^*)}{(\xi, \eta, \zeta)} \tag{17}$$

The viscous vectors are defined as

$$\hat{E}_V = \frac{1}{J}\begin{bmatrix} 0 \\ \xi_X\tau_{XX} + \xi_Y\tau_{XY} + \xi_Z\tau_{XZ} \\ \xi_X\tau_{XY} + \xi_Y\tau_{YY} + \xi_Z\tau_{YZ} \\ \xi_X\tau_{XZ} + \xi_Y\tau_{YZ} + \xi_Z\tau_{ZZ} \end{bmatrix}$$

$$\hat{F}_V = \frac{1}{J}\begin{bmatrix} 0 \\ \eta_X\tau_{XX} + \eta_Y\tau_{XY} + \eta_Z\tau_{XZ} \\ \eta_X\tau_{XY} + \eta_Y\tau_{YY} + \eta_Z\tau_{YZ} \\ \eta_X\tau_{XZ} + \eta_Y\tau_{YZ} + \eta_Z\tau_{ZZ} \end{bmatrix} \tag{18}$$

$$\hat{G}_V = \frac{1}{J}\begin{bmatrix} 0 \\ \zeta_X\tau_{XX} + \zeta_Y\tau_{XY} + \zeta_Z\tau_{XZ} \\ \zeta_X\tau_{XY} + \zeta_Y\tau_{YY} + \zeta_Z\tau_{YZ} \\ \zeta_X\tau_{XZ} + \zeta_Y\tau_{YZ} + \zeta_Z\tau_{ZZ} \end{bmatrix}$$

and τ_{XX}, τ_{YY}, τ_{ZZ}, τ_{XY}, τ_{XZ}, τ_{YZ} are:

$$\begin{aligned}
\tau_{XX} &= \frac{2}{\mathrm{Re}}[\xi_X u^*_\xi + \eta_X u^*_\eta + \zeta_X u^*_\zeta] \\
\tau_{YY} &= \frac{2}{\mathrm{Re}}[\xi_Y v^*_\xi + \eta_Y v^*_\eta + \zeta_Y v^*_\zeta] \\
\tau_{ZZ} &= \frac{2}{\mathrm{Re}}[\xi_Z w^*_\xi + \eta_Z w^*_\eta + \zeta_Z w^*_\zeta] \\
\tau_{XY} &= \frac{1}{\mathrm{Re}}[\xi_Y u^*_\xi + \eta_Y u^*_\eta + \zeta_Y u^*_\zeta + \xi_X v^*_\xi + \eta_X v^*_\eta + \zeta_X v^*_\zeta] \\
\tau_{YZ} &= \frac{1}{\mathrm{Re}}[\xi_Z v^*_\xi + \eta_Z v^*_\eta + \zeta_Z v^*_\zeta + \xi_Y w^*_\xi + \eta_Y w^*_\eta + \zeta_Y w^*_\zeta] \\
\tau_{XZ} &= \frac{1}{\mathrm{Re}}[\xi_X w^*_\xi + \eta_X w^*_\eta + \zeta_X w^*_\zeta + \xi_Z u^*_\xi + \eta_Z u^*_\eta + \zeta_Z u^*_\zeta]
\end{aligned} \tag{19}$$

The new terms due to the Coriolis force are included in the governing equation as a source term:

$$\hat{S} = \frac{1}{J}\begin{bmatrix} 0 \\ -2\mathrm{Ro}\,w^* \\ 0 \\ 2\mathrm{Ro}\,u^* \end{bmatrix} \tag{20}$$

The method suggested by Chorin (1967), known as the artificial compressibility method, is used to link the continuity equation with the momentum equation. Using this formulation an artificial term, the time derivative of the artificial density, is added to the continuity equation as shown in equation (12). With the addition of this term, the resulting set of equations is a mixed set of hyperbolic-parabolic equations, which can be solved using a standard time-march approach. This artificial term vanishes for the steady-state solution, allowing the solution of incompressible, steady flow problems without affecting the accuracy of the results.

In an incompressible fluid, a disturbance in the pressure field causes waves, which travel at infinite speed. Waves of finite speed result when the artificial compressibility method is used. The magnitude of this speed depends on the pseudo-compressibility constant β. Ideally, the value of the pseudo-compressibility constant should be chosen as high as the algorithm allows, so that incompressibility is quickly recovered.

The coupled partial differential equations are represented as a coupled algebraic system of equations using finite differences. This algebraic system of equations is solved using the coupled strongly implicit procedure (CSIP) proposed by Stone (1968) and utilized by Vaidyanathan (1998). The convective terms are discretized by a third-order upwind scheme and a second-order central difference scheme is used for the viscous terms. Results are obtained marching in time until the following convergence criterion is satisfied:

$$\sqrt{\frac{\sum_{i,j,k=1}^{i_m,j_m,k_m}\sum_{n=1}^{n=4}\left|\dfrac{q_n^{m+1}-q_n^m}{q_{n,\mathrm{rms}}^{m+1}}\right|}{4(i_m)(j_m)(k_m)}} \le 5\times 10^{-6} \tag{21}$$

where m is the iteration level, n the variable index (u, v, w, P), q_n the scalar value of the variable (u, v, w, P), i_m, j_m and k_m are the number of grid points in the ξ, η and ζ directions, respectively, and $q_{n,\mathrm{rms}}$ the root mean square value of q_n.

Boundary conditions

Non-slip and non-penetration boundary conditions are used at the wall of the duct. Therefore, the associated boundary conditions are:

$$u = v = w = 0 \quad \text{at the wall} \tag{22}$$

The boundary condition used for pressure at the wall is the boundary layer approximation valid in a rotating frame of reference. This boundary condition requires that the normal gradient of the modified pressure at the wall vanishes. The boundary layer approximation used in this work is

$$(\nabla P^*)\cdot\hat{n} = 0 \tag{23}$$

where P^* is the modified pressure and $\hat{n}$ is a unit vector normal to the surface.

At the inlet (Figure 1), the velocity profile is specified. For the cases presented in this study, the velocity profile for a fully developed flow in a straight duct is used. The fully developed straight-duct velocity profile under rotation is obtained using two different methods: (a) the streamfunction–vorticity method used by Speziale (1982); and (b) the three-dimensional CSIP solver developed in this work. It was found that both methods predict the same velocity profile at the inlet as shown in Section 4. However, the method of Speziale is preferred because less computational time is needed. This method is fully discussed in Speziale (1982, 1986). The pressure at the inlet is extrapolated from internal nodes.

At the outlet, the velocity profile is extrapolated from the internal nodes and therefore, a pressure boundary condition is needed at the outlet. It was found in this work that imposing constant pressure at the outlet was not accurate, particularly at high rotation numbers because the Coriolis force due to rotation produces a pressure gradient along the outlet surface. This problem is solved using the boundary condition proposed by Schiesser (1996). The pressure at the outlet is specified using the convective and Coriolis terms from the transverse momentum equations. The viscous terms are neglected because at moderate to high Reynolds numbers the hyperbolic derivatives are dominant. The y-momentum and z-momentum equations used for the pressure boundary condition at the outlet are:

$$u^* \frac{\partial v^*}{\partial x^*} + v^* \frac{\partial v^*}{\partial y^*} + w^* \frac{\partial v^*}{\partial z^*} = -\frac{\partial P^*}{\partial y^*} \tag{24}$$

$$u^* \frac{\partial w^*}{\partial x^*} + v^* \frac{\partial w^*}{\partial y^*} + w^* \frac{\partial w^*}{\partial z^*} = -\frac{\partial P^*}{\partial z^*} + 2\mathrm{Ro}\, u^* \tag{25}$$

Taking the derivative of equation (24) with respect to y^* and the derivative of equation (25) with respect to z^*, the following set of equations is obtained:

$$\frac{\partial^2 P^*}{\partial {y^*}^2} = \frac{\partial}{\partial y^*}(S_y) \quad \text{where} \quad S_y = -\left(u^* \frac{\partial v^*}{\partial x^*} + v^* \frac{\partial v^*}{\partial y^*} + w^* \frac{\partial v^*}{\partial z^*}\right) \tag{26}$$

and

$$\frac{\partial^2 P^*}{\partial {z^*}^2} = \frac{\partial}{\partial z^*}(S_z) \quad \text{where} \quad S_z = -\left(u^* \frac{\partial w^*}{\partial x^*} + v^* \frac{\partial w^*}{\partial y^*} + w^* \frac{\partial w^*}{\partial z^*}\right) + 2\mathrm{Ro}\, u^* \tag{27}$$

Adding equations (26) and (27), the following Poisson equation for pressure is obtained:

$$\frac{\partial^2 P^*}{\partial {y^*}^2} + \frac{\partial^2 P^*}{\partial {z^*}^2} = \frac{\partial}{\partial y^*}(S_y) + \frac{\partial}{\partial z^*}(S_z) \tag{28}$$

The source terms, S_y and S_z, are computed from the previous iteration level. Equation (25) is an elliptic partial differential equation and is solved using the line Gauss-Seidel iteration method proposed by Hoffman and Chiang (1995). This boundary condition yielded the pressure at the outlet and was successfully implemented in the CSIP/artificial compressibility code developed in this work. Papa (2000) showed that a developing laminar flow, within straight orthogonal rotating channels, could be considered fully developed at a distance three times its characteristic length. These results allow us to conclude that any disturbance effect of the outlet is minimized by placing this section at a distance five times its characteristic length.

Computations are performed on a $51 \times 21 \times 21$ (ξ by η by ζ) grid for the 180° bend with a circular cross-section or a square cross-section, where the aspect ratio is 1. Calculations with a rectangular cross-section and an aspect ratio of 2 are performed on a $51 \times 41 \times 21$ (ξ by η by ζ) grid. Results using a finer mesh, $101 \times 41 \times 41$, were obtained to check that the results were grid independent. The streamwise velocity is used as the parameter to check for grid independence. Figure 4 is a comparison of the streamwise velocity profile at three different angular locations along the 180° bend at the symmetry plane ($y = 0.0$) using the square cross-section with a $\mathrm{Re} = 200$ and two different rotation numbers ($\mathrm{Ro} = 0.0$ and $\mathrm{Ro} = 0.4$), under positive rotation. Equivalent results were obtained for the streamwise velocity comparison for an aspect ratio of 2 with the $51 \times 41 \times 21$ grid, and also for a circular cross-section duct. These results show that a grid definition of $51 \times 21 \times 21$ for the bend with either a circular or a square cross-section (aspect ratio of 1) is acceptable, and that the same is true when a grid of $51 \times 41 \times 21$ is used for the bend with a rectangular cross-section having an aspect ratio of 2.

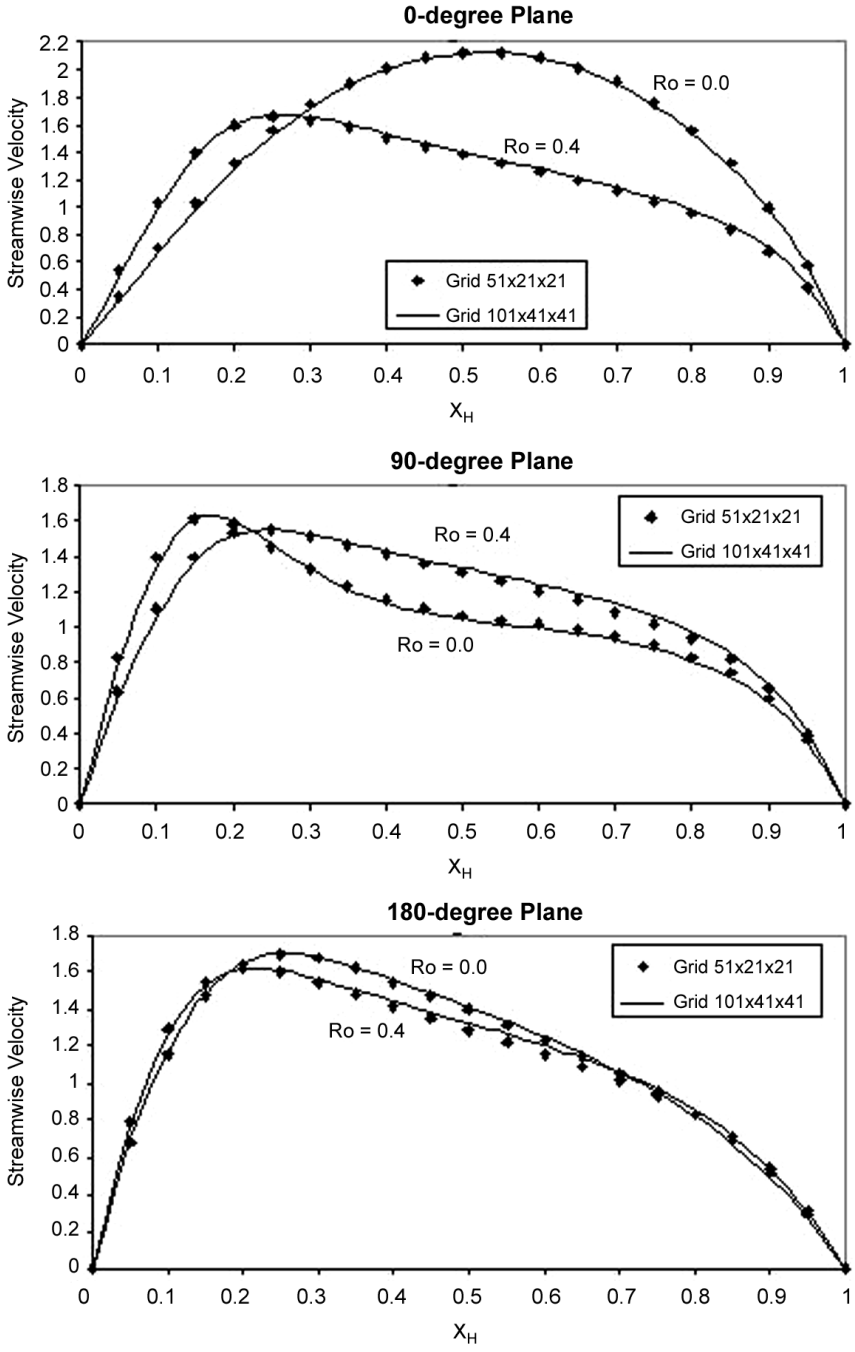

Figure 4.
Development of main flow in a 180° bend with square cross-section (Re = 200)

Results and discussion

Before discussing the predicted results for the flow in the rotating 180° bend, the validity of the numerical method used in this work is confirmed by comparing the predictions with the experimental results obtained by Akiyama *et al.* (1983). Figure 5 shows the axial velocity profile obtained in the present work and the experimental results obtained by Akiyama *et al.* for a 180° bend with a circular cross-section at Re = 1,000, Dean Number (K) = 666 and Ro = 0.0, i.e. no rotation. Very good agreement is evident at the 0° and 180° planes and good agreement is shown at the 90° plane.

The fully developed straight-duct velocity profile imposed at the inlet is obtained, as previously discussed, using the streamfunction–vorticity method proposed by Speziale (1982). The basis for this is shown in Figure 6(a) and (b), which contain the fully developed axial velocity contours for a straight duct with a square cross-section for Re = 100 and Ro = 0.1. As can be seen from the streamfunction–vorticity method, Figure 6(a), and the CSIP code developed in this work, Figure 6(b), produce virtually the same contours. The secondary flow produced by rotation is compared using both the methods in Figure 6(c) and (d). At higher Reynolds and rotation numbers, Speziale (1982) found that these two counter-rotating vortices break into four vortices. This behavior is also obtained in this work, as shown in Figure 7(a) and (b). This four-vortex regime was not found in the circular duct under rotation. The main advantage of the Speziale (1982) method is that the results are obtained using a two-dimensional analysis and assuming that the flow is fully developed in the axial direction. Therefore, a relatively coarse mesh containing only 21×21 nodes can be used for the calculations. This compares to a mesh containing $51 \times 21 \times 21$ nodes used by the CSIP code.

The evolution of the streamwise velocity in a 180° bend with a circular cross-section for Re = 200 under positive or negative rotation is shown in Figure 8(a) and (b), respectively. Under positive rotation the force due to the curvature of the bend and the Coriolis force are acting outwards. Therefore, the streamwise velocity along the inlet, bend and outlet sections is higher closer to the outer wall. Under negative rotation, the streamwise velocity along the inlet and outlet sections is higher closer to the inner wall because the Coriolis force is acting inwards. However, along the bend the centrifugal force due to the curvature is acting outwards and overcomes the Coriolis force, pushing the streamwise flow towards the outer wall.

Tables I, II and III show the maximum magnitude of the secondary flow velocity for the 180° bend for a range of Dean and rotation numbers using circular, square and rectangular cross-sections, respectively. The maximum absolute value for the secondary flow along the bend at the same Dean number, K, is found to be for Ro = 0.0, i.e. the non-rotating cases. This behavior is obtained for all cross-sections used in this study. These results are interesting because they show that the magnitude of the secondary flow along a bend is

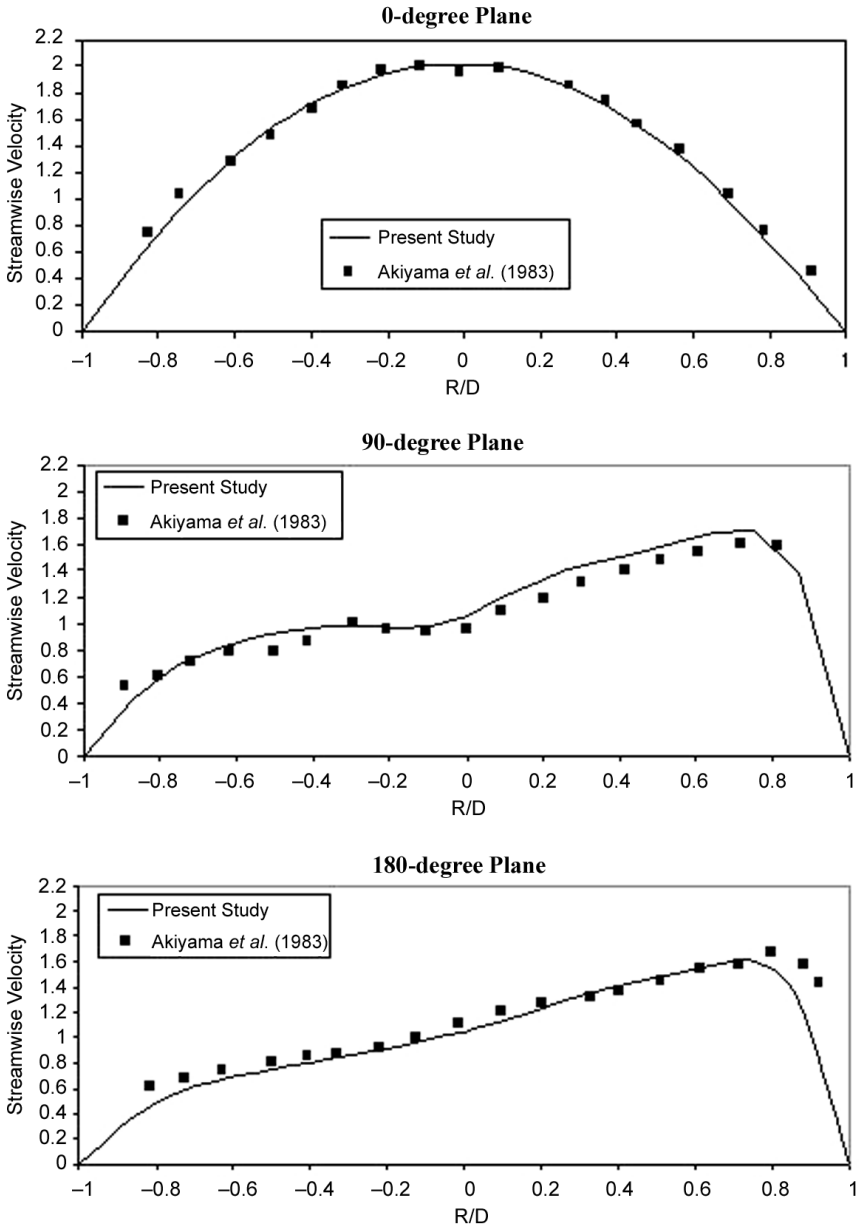

Figure 5.
Development of main flow in a 180° bend with circular cross-section for Re = 1,000, $K = 666$ and Ro = 0.0

decreased under either positive or negative rotation. Positive rotation does not increase the secondary flow along the bend because the streamwise flow before entering the bend is closer to the outer wall, as shown in Figure 8(a). In addition, secondary flow along the bend for higher Dean numbers is decreased

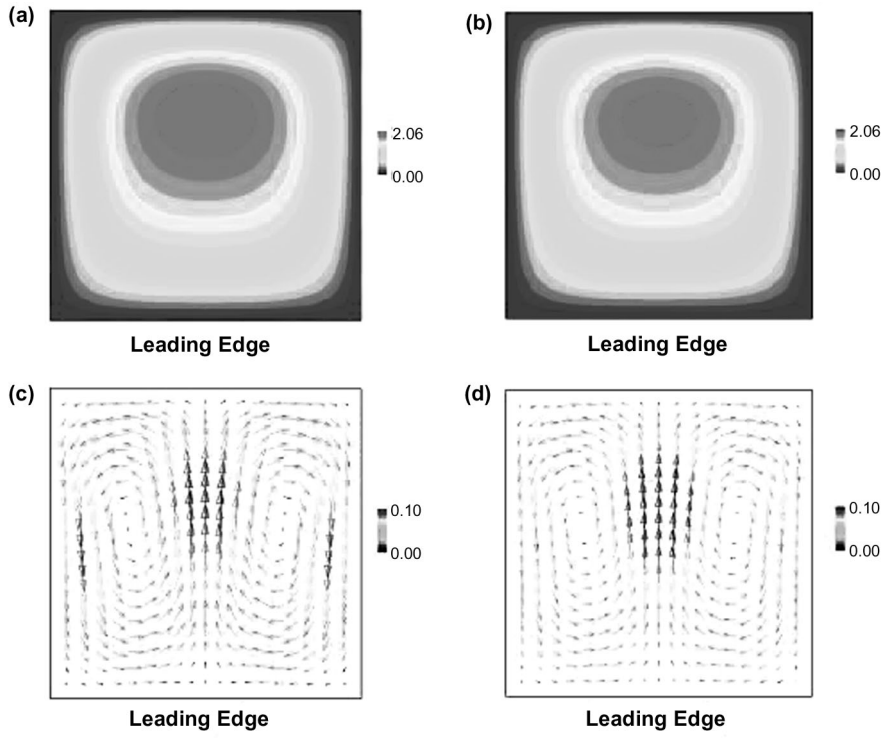

Figure 6.
(a) Inlet axial velocity contour using the vorticity–streamfunction method; (b) inlet axial velocity contour using the 3-D CSIP code; (c) inlet secondary flow using the vorticity–streamfunction method; (d) inlet secondary flow using the 3-D CSIP code (Re = 100, Ro = 0.1)

substantially under negative rotation because the Coriolis force acts in a direction opposite to the centrifugal force produced by the curvature of the bend. The secondary flow pattern along the bend with a circular cross-section can be described mainly by the formation of two counter-rotating vortices. Figure 9(a) and (b) shows the secondary flow pattern for the circular 180° bend at the same angular location (180° plane), Ro = 0.0 (no-rotation) and Ro = 0.2 (positive rotation), respectively. The figure shows that the rotation decreases the strength or magnitude of this pair of counter-rotating vortices (shorter vector length) but does not change their position.

For rectangular bends, the two counter-rotating vortices break into four vortices if the Dean number is higher than a critical value. Yang and Ye (1996), Ghia and Sokhey (1977), and Daskopoulos and Lenhoff (1989) have previously reported this complex four-vortex formation before for non-rotating bends. For the present study, Figure 10(a) and (b) shows the two counter-rotating flow patterns at the exit of the bend for the non-rotating rectangular duct with two different aspect ratios for a Dean number of 132, and Figure 10(c) and (d) shows the four vortices formation for a Dean number of 264. This pattern of secondary

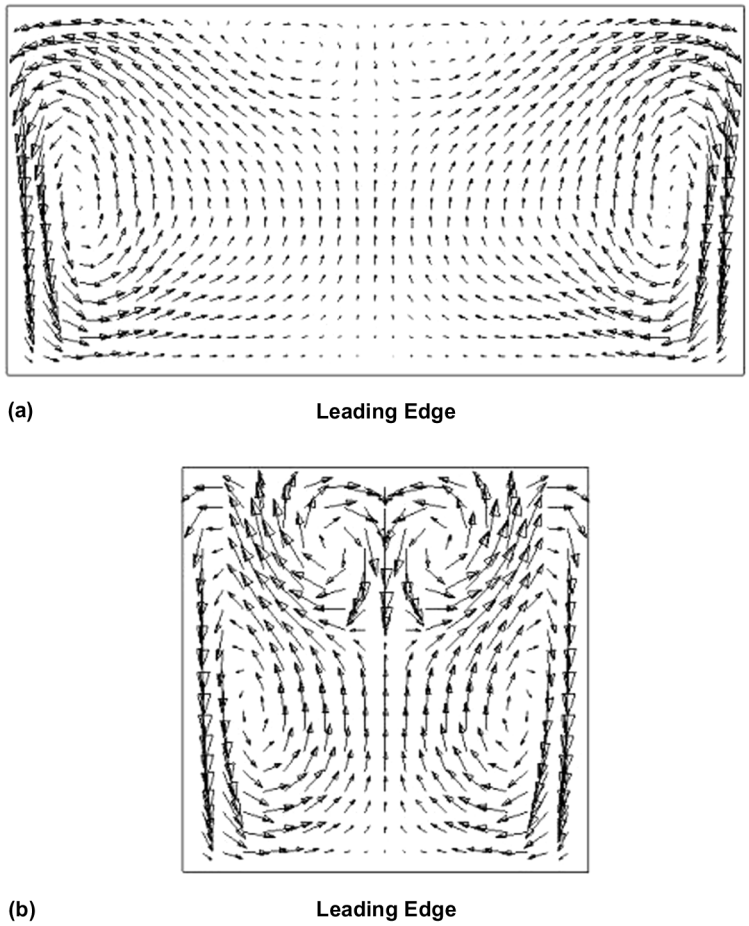

Figure 7.
(a) Inlet secondary flow pattern in a rotating rectangular duct with an aspect ratio of 2; (b) inlet secondary flow pattern in a rotating rectangular duct with an aspect ratio of 1 (Re = 400 and Ro = 0.2)

flow was not observed for the circular bend in the range of Dean numbers used in this work.

Conclusion

The developing laminar flow within a rotating 180° bend with three different cross-sections is studied via the finite difference method using a boundary fitted coordinate system and the artificial compressibility method. The effect of rotation on the flow is considered in the complete Navier–Stokes equations by the addition of Coriolis and centrifugal forces. Two new boundary conditions are successfully used in this work: determination of the fully developed straight duct inlet flow velocity profile under rotation and the correct specification of the outlet boundary condition for pressure.

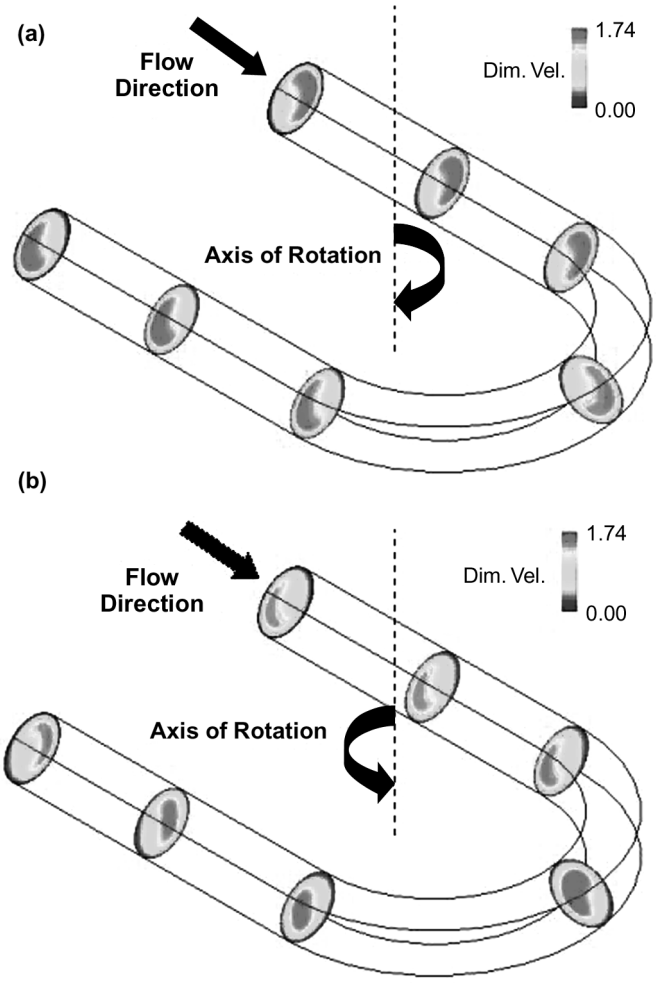

Figure 8.
(a) Steam-wise velocity contour under positive rotation (Re = 200, Ro = 0.4); (b) stream-wise velocity contour under negative rotation (Re = 200, Ro = 0.4)

Table I.
Maximum secondary velocity for the circular 180° bend

	Positive rotation		No rotation	Negative rotation	
K	Ro = 0.2	Ro = 0.4	Ro = 0.0	Ro = 0.2	Ro = 0.4
65.94	0.3224	0.3095	0.4113	0.3362	0.3164
131.88	0.3293	0.3354	0.4705	0.2928	0.3091
263.75	0.3242	0.3231	0.5038	0.3054	0.3155

The present analysis reveals that the effects of rotation on the flow behavior in straight or curved ducts is quite complex. Regardless of duct geometry, rotation causes secondary flows to occur which consist of a pair of counter-rotating vortices, similar to the secondary flow pattern in a curved bend without rotation. For high Reynolds and rotation numbers, these patterns in rectangular ducts can break into two or more pair of vortices.

For the flow in a rotating duct having a 180° bend, regardless of cross-section, positive rotation results in the maximum streamwise velocity being located closer to the outer wall in all sections of the duct since both the centrifugal and Coriolis forces act outward. For negative rotation, the Coriolis force acts inward and the location of the maximum streamwise velocity is

	Positive rotation		No rotation	Negative rotation	
K	Ro = 0.2	Ro = 0.4	Ro = 0.0	Ro = 0.2	Ro = 0.4
65.94	0.3670	0.3521	0.4853	0.3798	0.3480
131.88	0.3819	0.3749	0.5567	0.2820	0.3286
263.75	0.4454	0.3402	0.6987	0.3022	0.3224

Table II. Maximum secondary velocity for the square 180° bend

	Positive rotation		No rotation	Negative rotation	
K	Ro = 0.1	Ro = 0.2	Ro = 0.0	Ro = 0.1	Ro = 0.2
65.94	0.4550	0.4417	0.4729	0.3827	0.2986
131.88	0.4440	0.4279	0.6446	0.4086	0.2974
263.75	0.4321	0.5538	0.7816	0.3845	0.2571

Table III. Maximum secondary velocity for the rectangular 180° bend with an aspect ratio of 2

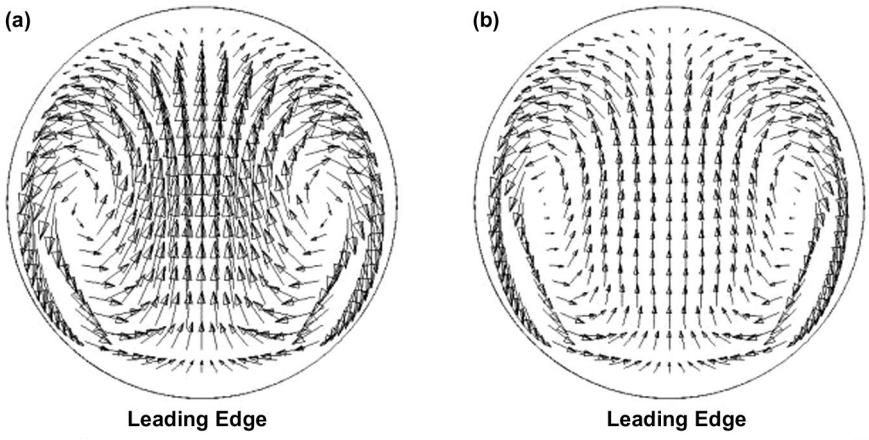

Figure 9. (a) Secondary flow pattern at the bend outlet for the circular geometry (Re = 200, Ro = 0.0); (b) secondary flow pattern at the bend outlet for the circular geometry (Re = 200 and Ro = 0.2)

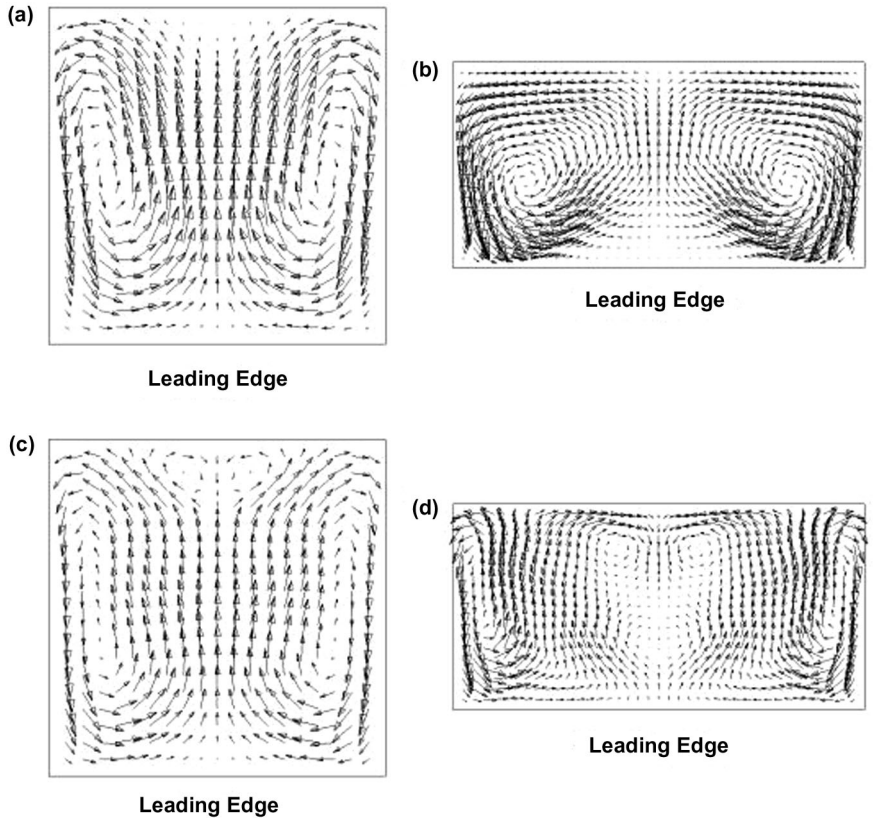

Figure 10.
(a) Secondary flow pattern for the square 180° bend ($K = 132$, $\mathrm{Re} = 200$ and $\mathrm{Ro} = 0.0$). (b) Secondary flow pattern for the rectangular 180° bend with an aspect ratio of 2 ($K = 132$, $\mathrm{Re} = 200$ and $\mathrm{Ro} = 0.0$). (c) Secondary flow pattern for the square 180° bend ($K = 264$, $\mathrm{Re} = 400$ and $\mathrm{Ro} = 0.0$). (d) Secondary flow pattern for the rectangular 180° bend with an aspect ratio of 2 ($K = 264$, $\mathrm{Re} = 400$ and $\mathrm{Ro} = 0.0$)

along the inner wall in the inlet and outlet sections, but is closer to the outer wall in the bend. Interestingly, the strength of the secondary flow in the 180° bend due to both curvature and rotation, either positive or negative, decreases as compared to the vortex strength for no rotation.

References

Akiyama, M., Hanaoka, Y., Cheng, K.C., Urai, I. and Suzuki, M. (1983), "Visual measurements of laminar flow in the entry region of a curved pipe", in Yang, W.J. (Ed.), *Proceedings of the Third International Symposium on Flow Visualization*, Hemisphere Publishing Corporation, New York, pp. 526-30.

Barua, S.N. (1955), "Secondary flow in a rotating straight pipe", *Proceedings of the Royal Society of London*, Vol. 227, pp. 133-9.

Benton, G.S. (1956), "The effects of the earth's rotation on laminar flow in pipes", *ASME Journal of Applied Mechanics*, Vol. 23, pp. 123-7.

Chorin, A.J. (1967), "A numerical method for solving incompressible viscous flow problems", *Journal of Computational Physics*, Vol. 2, pp. 12-26.

Daskopoulos, P. and Lenhoff, A.M. (1989), "Flow in curved ducts: bifurcation structure for stationary ducts", *Journal of Fluid Mechanics*, Vol. 203, pp. 125-48.

Daskopoulos, P. and Lenhoff, A.M. (1990), "Flow in curved ducts. Part 2. Rotating ducts", *Journal of Fluid Mechanics*, Vol. 217, pp. 575-93.

Dean, W.R. (1928), "The streamline motion of fluid in a curved pipe", *Philosophy Magazine*, Vol. 5, pp. 673-95.

Ghia, K.N. and Sokhey, J.S. (1977), "Laminar incompressible viscous flow in curved ducts of regular cross-sections", *Journal of Fluids Engineering*, Vol. 99, pp. 640-8.

Hoffman, K.A. and Chiang, S.T. (1995), "Computational fluid dynamics for engineers", in, *Publication of Engineering Education System*, Wichita, KA, USA, pp. 154-77.

Hwang, J.J. and Lai, D.Y. (1998a), "Three-dimensional mixed convection in a rotating multiple-pass square channel", *International Journal of Heat and Mass Transfer*, Vol. 41, pp. 979-91.

Hwang, J.J. and Lai, D.Y. (1998b), "Three-dimensional laminar flow in a rotating multiple pass square channel with sharp 180-deg turns", *Journal of Fluids Engineering*, Vol. 120, pp. 488-95.

Iacovides, H., Launder, B.E. and Li, H.-Y. (1996), "The computation of flow development through stationary and rotating U-ducts of strong curvature", *International Journal of Heat and Fluid Flow*, Vol. 17, pp. 22-33.

Ito, H. and Motal, T. (1974), "Secondary flow in a rotating curved pipe", Reports from The Institute of High Speed Mechanics, Tohoku University, Vol. 29, pp. 33–57.

Papa, F. (2000), "Confined flow simulation for a non-inertial frame of reference", Doctoral Dissertation in Chemical Engineering, University of Toledo, Toledo, OH.

Schiesser, W.E. (1996), "PDE boundary conditions from minimum reduction of the PDE", *Applied Numerical Mathematics*, Vol. 20, pp. 171-9.

Selmi, M., Nandakumar, K. and Finlay, W.H. (1994), "A bifurcation study of viscous flow through a rotating curved duct", *Journal of Fluid Mechanics*, Vol. 262, pp. 353-75.

Speziale, C.G. (1982), "Numerical study of viscous flow in rotating rectangular ducts", *Journal of Fluid Mechanics*, Vol. 122, pp. 251-71.

Speziale, C.G. (1986), "The effect of the earth's rotation on channel flow", *Journal of Applied Mechanics*, Vol. 53, pp. 198-202.

Stone, H.L. (1968), "Iterative solution of implicit approximations of multi-dimensional partial differential equations", *SIAM Journal on Numerical Analysis*, Vol. 5, pp. 530-58.

Vaidyanathan, K. (1998), "Coupled strongly implicit Navier–Stokes computation using artificial compressibility formulation for incompressible internal flow problems", Doctoral Dissertation in Mechanical Engineering, University of Toledo, Toledo, OH.

Yang, Z. and Ye, R. (1996), "Symmetry-breaking and bifurcation study on the laminar flows through curved pipes with a circular cross-section", *Journal of Computational Physics*, Vol. 127, pp. 73-87.